THE JOURNAL OF PHYSICAL CHEMISTRY C

Article

Cite This: J. Phys. Chem. C 2019, 123, 14391−14397

pubs.acs.org/JPCC

Single Ru Sites-Embedded Rutile TiO_2 Catalyst for Non-Oxidative Direct Conversion of Methane: A First-Principles Study

Xiufang Ma,[†] Keju Sun,[‡] Jin-Xun Liu,[§,#] Wei-Xue Li,[∥,⊥] Xingmin Cai,[†] and Hai-Yan Su*[,§]

[†]Shenzhen Key Laboratory of Advanced Thin Films and Applications, College of Physics and Optoelectronic Engineering, Shenzhen University, Shenzhen 518060, P. R. China

[‡]Key Laboratory of Applied Chemistry, College of Environmental and Chemical Engineering, Yanshan University, 438 Hebei Avenue, Qinhuangdao 066004, P. R. China

[§]State Key Laboratory of Molecular Reaction Dynamics, Dalian Institute of Chemical Physics, Chinese Academy of Science, Dalian 116023, P. R. China

[∥]Department of Chemical Physics, School of Chemistry and Materials Science, iChEM, University of Science and Technology of China, Hefei 230026, P. R. China

[⊥]CAS Excellence Center for Nanoscience, Hefei National Laboratory for Physical Sciences at Microscale, Hefei 230026, P. R. China

Supporting Information

ABSTRACT: Non-oxidative direct methane conversion provides a potentially economic and environmental friendly route for the use of natural gas and shale gas, but this process suffers the disadvantages of low activity and selectivity and harsh operating conditions. Using density functional calculations, we develop the relations in heats of adsorption of CH_x (x = 0−4) species and catalytic performance of conventional Fe, Ru, and Co-based catalysts and identify the key factors that affect the activity and selectivity as methane adsorption and the relative strength of CH_2 and CH adsorption. Based on the analysis, we design the single Ru sites embedded in rutile TiO_2(110) catalyst, which tunes the adsorption strength of CH_x compared with the traditional Ru-based catalyst, particularly weakening CH adsorption relative to CH_2 adsorption, thus leading to increased activity, improved selectivity toward ethylene, and strong resistance toward coking. This work highlights the impact of surface coordination environment, achieving fundamental insight that can be used to design and develop improved catalysts for direct methane conversion and other important reactions of technological interest.

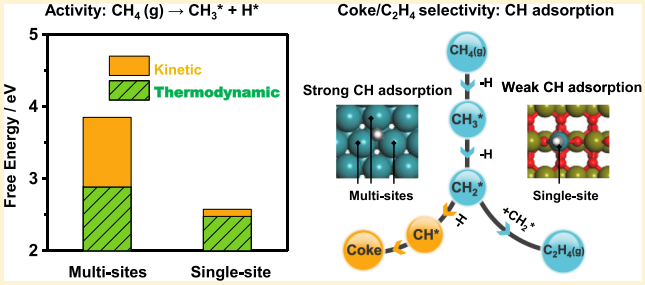

1. INTRODUCTION

The abundance of natural gas and the advances in the extraction technology of shale gas makes methane a valuable raw material for the petrochemical industry.[1,2] Compared to the multistage methane conversion via syngas (a mixture of H_2 and CO), the direct conversion of methane provides a potentially more economical and environmental-friendly route for carbon resource utilization.[2−5] In particular, the non-oxidative direct conversion of methane, which avoids the generation of side products such as CO_2 and CO as in the direct oxidative conversion, can increase the carbon-atom utilization efficiency in principle.[2−5] Recently, Bao et al. reported that the single-iron sites embedded in a silica matrix can activate methane in the absence of oxidants, producing ethylene, aromatics, and hydrogen as the only products, with ethylene dominating at short space-times for a selectivity of ∼52.7% at 1293 K.[6]

Although the enormous progresses have been achieved with non-oxidative direct conversion of methane experimentally,[2−8] two fundamental problems still need to be understood for highly efficient methane conversion. First, the reactivity of catalyst is very poor at low temperatures.[3,9,10] For instance, methane conversion is only 11.5% on the Mo-based catalysts at 983 K.[7] To achieve a higher conversion rate, elevated temperatures (>1100 K) are often employed.[6,8] It is generally believed that the scission of the first C−H bond limits the total activity of methane conversion. However, it remains unclear why the first C−H bond is so difficult to be activated and how to facilitate its activation. Second, coking is often produced at the operating conditions (973−1123 K) for non-oxidative direct conversion of methane, which causes the degradation in selectivity and stability.[9,11−13] Mechanistically, once the first C−H bond is cleaved, the subsequent dehydrogenation on the surface of transition metal catalysts is quite facile, leading to the formation of coke eventually.[14,15] Therefore, the challenge for improved activity, selectivity, and stability is to tune the

Received: February 21, 2019
Revised: May 20, 2019
Published: May 22, 2019

DOI: 10.1021/acs.jpcc.9b01638
J. Phys. Chem. C 2019, 123, 14391−14397

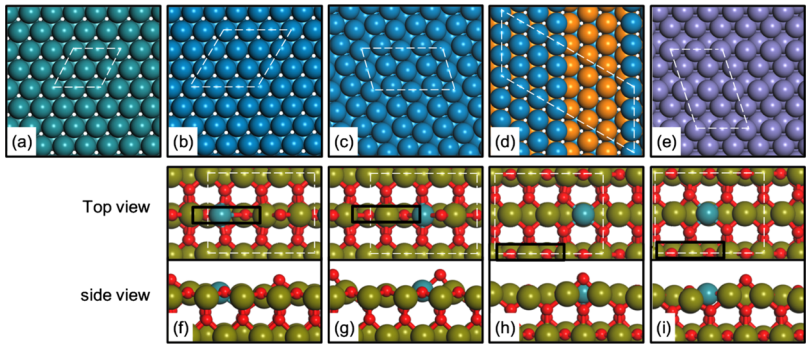

Figure 1. Schematic structures for various metals (top view) and $Ru_1/TiO_2(110)$ surfaces (top and side views). (a) Ru(0001), (b) Co(0001), (c) Co(10$\bar{1}$1), (d) stepped Co, (e) Fe(310), $Ru_1/TiO_2(110)$, where Ru coordinates with two (f) or one (g) bridge O_v and where Ru substitutes a five-coordinated Ti with (h) or without (i) bridge O at the nearest neighbor. The cyan, blue, purple, dark yellow, and red balls represent Ru, Co, Fe, Ti, and O atom, respectively. The unit cells are denoted by the dashed white lines and the bridge O_v pairs on $Ru_1/TiO_2(110)$ are highlighted in black rectangle.

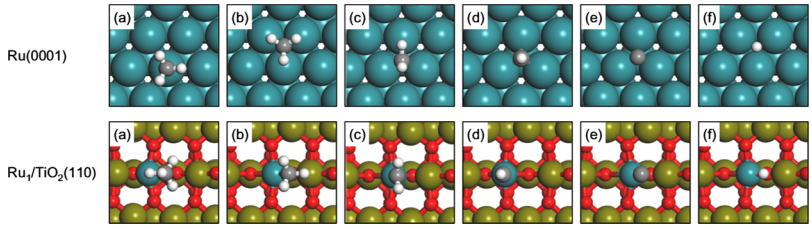

Figure 2. Preferred adsorption configurations of (a) CH_4, (b) CH_3, (c) CH_2, (d) CH, (e) C, and (f) H on Ru(0001) and $Ru_1/TiO_2(110)$ surfaces. The cyan, dark yellow, gray, white, and red balls represent Ru, Ti, C, H, and O atom, respectively.

relative reaction rates of the different methane dehydrogenation steps (facilitate the first step whereas retard the last steps) by changing catalyst structure and composition.[16,17]

Using density functional theory (DFT) calculations, we identify the key factors that control the activity, selectivity, and stability toward the non-oxidative direct conversion of methane to ethylene on the conventional transition metal (such as Fe, Ru, and Co) surfaces. Guided by the fundamental understanding, we design the single Ru sites embedded in a rutile $TiO_2(110)$ matrix [denoted by $Ru_1/TiO_2(110)$] to tune the adsorption strength of CH_x (x = 0−4) by coordination environment and synergistic effect, achieving improved methane conversion activity, ethylene selectivity, and coking resistance.

2. COMPUTATIONAL METHODS

Spin-polarized DFT calculations were carried out for all the systems except Ru(0001) using VASP5.3,[18,19] with the all-electron projector augmented wave method.[20,21] The exchange-correlation effects were described by the generalized gradient approximation in form of Perdew−Burke−Ernzerhof.[22] The wave functions were expanded in a basis of plane waves with a kinetic energy cutoff of 400 eV and a density cutoff of 900 eV. The calculated lattice constants for bulk Ru, Co, Fe, and rutile TiO_2 were 2.72 Å/4.29 Å, 2.50 Å/4.03 Å, 2.83 Å, and 4.65 Å/2.97 Å, respectively, which agrees well with the experiments (2.71 Å/4.28 Å, 2.51 Å/4.07 Å, 2.87 Å, and 4.59 Å/2.96 Å).[23,24]

The Ru(0001) surface was modeled by a five-layer slab with the (2 × 2) periodicity. The Co(0001) and Co(10$\bar{1}$1) surfaces were modeled using a four-layer slab within (3 × 3) and (2 × 2) surface unit cells, respectively. The stepped Co surface was modeled using a four-layer (7 × 3) close-packed surface, in which three neighboring rows of metal atoms on the top layer are removed. The stepped Fe(310) surface was modeled by a slab with four equivalent Fe(110) layers, and a (2 × 2) unit cell was chosen. The single Ru sites embedded in a rutile $TiO_2(110)$ [$Ru_1/TiO_2(110)$] was modeled by a four O−Ti−O trilayer slab with the (3 × 1) periodicity, where one-sixth of the surface Ti atoms were substituted by Ru atoms (see Supporting Information for more details of the model). The structures for the simulated surfaces are shown in Figure 1. A vacuum region of 15−16 Å was used along the z-direction to avoid the interactions between repeated slabs. The surface Brillouin zone was sampled by (6 × 6 × 1), (4 × 4 × 1), (5 × 5 × 1), (4 × 2 × 1), (5 × 5 × 1), and (4 × 6 × 1) Monkhorst−Pack grid meshes for the Ru(0001), Co(0001), Co(10$\bar{1}$1), stepped Co, Fe(310), and $Ru_1/TiO_2(110)$ surface, respectively.[25] The adsorbates and the top two metal or TiO_2 layers were fully relaxed till the residual forces were less than 0.03 eV/Å, while the remained layers were fixed to their bulk truncated position.

The adsorption energy ΔE_{ads} was calculated to be the energy gain of the adsorption with respect to the clean substrates and corresponding species in the gas phase. Here, a positive (negative) value indicates that the adsorption is endothermic (exothermic). The adsorption free energy ΔG of methane was obtained by $\Delta G = \Delta E_{ads} + \Delta ZPE - T\Delta S$, where ΔE_{ads}, T, ΔZPE, and ΔS were the adsorption energy of methane, temperature, the change in zero-point energy, and entropy due to the adsorption, respectively. ZPE values of gaseous and adsorbed methane were obtained by DFT calculated frequencies, and S of gaseous methane was obtained by standard tables.[23] The transition states (TSs) were located by the climbing-image nudged elastic band method[26,27] and force reversed method[28] and confirmed by frequency analysis. The relaxations were stopped when the residual forces were less

DOI: 10.1021/acs.jpcc.9b01638
J. Phys. Chem. C 2019, 123, 14391−14397

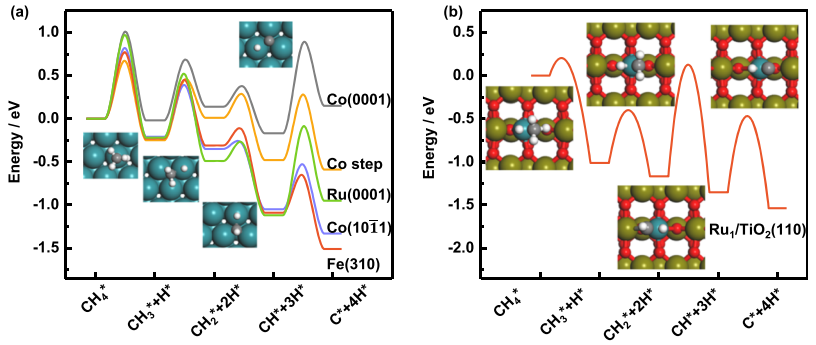

Figure 3. Energy profiles of methane dehydrogenation on (a) pure metals and (b) $Ru_1/TiO_2(110)$. The transition state structures on Ru(0001) and $Ru_1/TiO_2(110)$ are given. The cyan, dark yellow, gray, white, and red balls represent Ru, Ti, C, H, and O atom, respectively.

than 0.03 eV/Å. The activation energies (ΔE_{act}) and reaction heat (ΔH) were calculated with respect to the most stable state for separate adsorption of adsorbates on the surfaces. Zero-point energy corrections were not included in ΔE_{act} calculation.

3. RESULTS AND DISCUSSION

3.1. Methane Dehydrogenation on the Conventional Transition Metal Catalysts. We first study methane dehydrogenation on the conventional transition metal catalysts, including Fe(310), Ru(0001), Co(0001), stepped Co, and Co(10$\bar{1}$1) surfaces. The adsorption energies ΔE_{ads} of the various intermediates at the most stable sites (Figures 2 and S1) are listed in Table S1, and the energy profiles are presented in Figure 3a. Regardless of the nature and structure of transition metals, two main features can be found from Figure 3a: (1) when using the adsorbed methane (CH_4^*) as the energy reference, the scission of the first C−H bond that has been believed to be the rate-limiting step of direct methane conversion is not too difficult. The reaction is modestly exothermic by 0.03−0.25 eV, with the activation energy ΔE_{act} of at most 1.01 eV (Table S2). (2) CH or C has the lowest energy among the CH_x (x = 0−3) intermediates in the energy profile, which is thermodynamically more favorable for the formation of coke instead of ethylene. For the latter one, the preferred CH_x intermediate should be CH_3 or CH_2. Furthermore, compared to other dehydrogenation steps, CH_2 dehydrogenation has substantially lower barrier (ΔE_{act} = 0.03−0.26 eV). The ΔE_{act} for CH_2 dehydrogenation is also much lower than its dimerization on the surfaces studied, typically falling in the range of 0.37−1.23 eV,[29,30] indicative of facile coke formation kinetically. Our calculated CH_x (x = 1−4) dehydrogenation barriers on Ru(0001), Co(0001), and stepped Co agree well with previous DFT studies by van Santen et al. and Hu et al., with ΔE_{act} differing by 0.02−0.23 eV.[14,31,32] The slight discrepancy may be explained by the different functionals and pseudopotentials used in our calculations and previous studies.

Because the first C−H bond scission is so facile kinetically, what factors lead to the low activity of direct methane conversion? Are they primarily thermodynamic or kinetic factors? To understand these questions, we considered the effect of entropy and zero point energy. Using the free energy of gaseous methane (CH_4(g)) and clean surfaces as the energy reference, we decompose the activation energy ΔE_{act2} of the first C−H bond scission into two terms

$$\Delta E_{act2} = \Delta E_{act1} + \Delta G$$

ΔE_{act1} and ΔG are the activation energy relative to adsorbed methane (CH_4^*) and adsorption free energy of methane, respectively. As shown in Figure 4, ΔE_{act2} of the first C−H

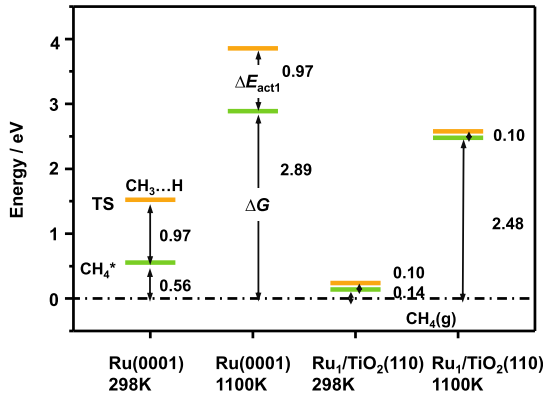

Figure 4. Activation energy decomposition for the first C−H bond scission in methane on Ru(0001) and $Ru_1/TiO_2(110)$ at 298 and 1100 K.

bond scission on Ru(0001) is calculated to be 1.53 eV at 298 K, much higher than ΔE_{act1} by 0.56 eV. The ΔG is positive, implying that CH_4(g) is more stable than CH_4^*. This can be well understood because no excess electrons or empty orbitals are available in the C atom of methane to bond with the surface. As the temperature increases, the effect of entropy becomes more significant, leading to more positive ΔG. At the temperature (T = 1100 K) where direct methane conversion to ethylene is thermodynamically feasible, ΔG is as high as 2.89 eV (with the contribution of entropy of 2.91 eV), which largely increases the difficulty of methane adsorption and dominates the total ΔE_{act2}. Therefore, the unfavorable thermochemistry is primarily responsible for the difficult methane activation in the non-oxidative coupling process of methane. The oxidants such as O_2 and so forth[33,34] have been introduced to the reaction process to overcome the thermodynamic limitation (more negative free energy change relative to the non-oxidative coupling of methane at the same temperature), which is the so-called oxidative coupling process of methane.

Having identified the key factors that affect the activity of direct methane conversion, we then turn our attention to the selectivity of ethylene and coking. As discussed above, to improve the selectivity of ethylene relative to coking on the transition metal catalysts, one key issue is to suppress CH_2 dehydrogenation. We will show below how this can be achieved by fundamental understanding guided material

DOI: 10.1021/acs.jpcc.9b01638
J. Phys. Chem. C 2019, 123, 14391−14397

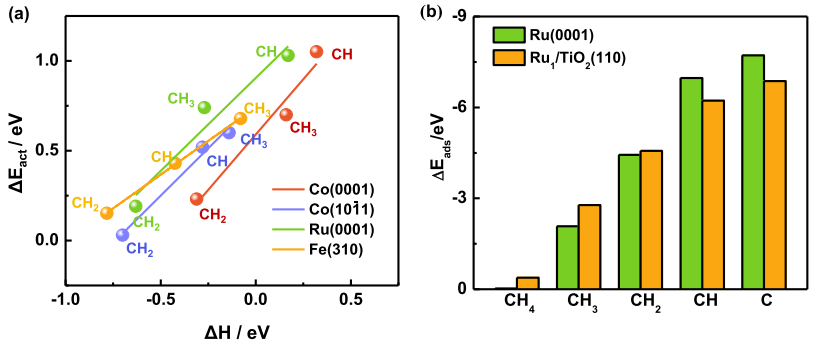

Figure 5. (a) Activation energies ΔE_{act} of CH_x (x = 1−3) dehydrogenation as a function of the reaction heat ΔH; (b) adsorption energies ΔE_{ads} of CH_x (x = 0−4) at the favorable sites on Ru(0001) and $Ru_1/TiO_2(110)$.

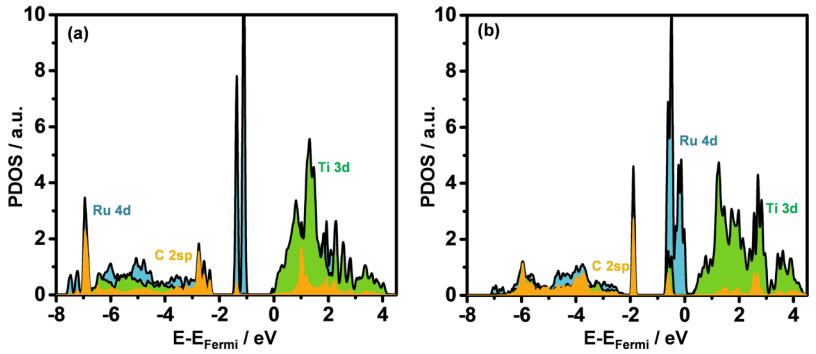

Figure 6. PDOS for adsorption of CH (a) and CH_2 (b) on $Ru_1/TiO_2(110)$. The PDOS of C 2sp, coordinated Ru 4d, and Ti 3d are represented by yellow, blue, and green areas, respectively. The reference zero is Fermi energy level.

design. Our calculations show that the structures of the initial states (ISs) and transition states (TSs) of CH_x (x = 1−3) dehydrogenation are very alike on Ru(0001), Co(0001), Co(10$\bar{1}$1), and Fe(310): CH_x generally adsorbs at the hollow site at the IS (Figures 2 and S1) and remains almost unchanged at the TS, with the dissociated H atom at the adjacent top (0001) or bridge site (10$\bar{1}$1 and 310), as shown in Figures 3a and S2. This leads to a good Brønsted−Evans−Polanyi relation between the ΔE_{act} and reaction heat ΔH of the CH_x (x = 1−3) dehydrogenation on these surfaces, as shown in Figure 5a, suggesting that the kinetics is largely determined by the thermochemistry. Correspondingly, CH_2 dehydrogenation and coke formation can be inhibited by weakening CH adsorption with respect to CH_2 adsorption.

3.2. Methane Dehydrogenation on the Single Ru Sites Embedded in TiO_2(110). In our previous work, we found that the coordination environment of metal had a significant effect on the relative adsorption strength of CH_x (x = 0−4). Specifically, compared to the stepped Ir with the Ir−Ir coordination, the single Ir sites embedded in the rutile $TiO_2(110)$, where Ir coordinates with O, weakened CH adsorption (by 1.68 eV) more than CH_2 adsorption (by 1.10 eV).[35] We thus choose the single Ru sites embedded in the rutile $TiO_2(110)$ (denoted by $Ru_1/TiO_2(110)$), with the hope to weaken CH adsorption with respect to CH_2 adsorption and in turn to improve the ethylene versus coke selectivity by the Ru−O coordination environment. Ru is chosen due to its high activity in methane activation and the high stability of $Ru_1/TiO_2(110)$ caused by the similar lattice distances between RuO_2 and rutile TiO_2.[36]

The bridge oxygen vacancy (O_v) on the $TiO_2(110)$ surface have been shown to play a crucial role for high activity in many catalytic reactions.[30,37] To simulate the coupling reaction of two methane molecules in the present work, two adjacent bridging O_v (O_v pairs) on $Ru_1/TiO_2(110)$ are required. The previous scanning tunneling microscopy experiment and DFT calculation have shown that the bridge O_v pairs are more stable than two discrete bridge O_v on pure $TiO_2(110)$.[38] We further study the effect of Ru doping on the bridge O_v arrangement in a (4 × 1) $TiO_2(110)$ unit cell. It is found that the bridge O_v pairs (Figure S3a) almost energetically degenerate with two discrete bridge O_v (Figure S3b), indicating that the bridge O_v pairs can also be stable on $Ru_1/TiO_2(110)$. To reduce the computational cost, we employ a (3 × 1) $TiO_2(110)$ unit cell to model the bridge O_v pairs and systematically study the effect of Ru locations in the following. There are four possible Ru locations: Ru atom coordinates with two (Figure 1f) or one bridge O_v (Figure 1g); Ru substitutes a five-coordinated Ti, with (Figure 1h) or without (Figure 1i) bridge O at the nearest neighbor. The configurations in Figure 1f,g are more stable than those in Figure 1h,i by 0.21−0.29 eV (Table S3). Therefore, the configuration in Figure 1f was finally chosen to model the $Ru_1/TiO_2(110)$.

Having determined the model for $Ru_1/TiO_2(110)$, we investigate the adsorption of intermediates involved in nonoxidative coupling process of methane. Various possible adsorption sites have been studied (Tables S4 and S5, Figure S4), and the most stable structures are shown in Figure 2. Interestingly, compared to Ru(0001), CH_2 binds on $Ru_1/TiO_2(110)$ slightly stronger by 0.14 eV, whereas CH binds largely weaker by 0.75 eV (Figure 5b). The projected densities of states (PDOS) for CH and CH_2 adsorption on the $Ru_1/TiO_2(110)$ surface are plotted in Figure 6. For both CH and CH_2 adsorption, the peak intensities of Ti-derived states are

DOI: 10.1021/acs.jpcc.9b01638
J. Phys. Chem. C 2019, 123, 14391−14397

very small, indicative of the weak hybridization between the two adsorbates and Ti. In contrast, the extensive hybridizations between C and Ru are found at energy windows of (−7.11, −6.73 eV) and (−2.90, −2.23 eV) for CH and those of (−6.43, −5.83 eV) and (−2.05, −1.73 eV) for CH_2, which can be attributed to the bonding states between CH/CH_2 and Ru. These results suggest that the adsorbates mainly bind with the single Ru sites on Ru_1/TiO_2, and the weakened CH adsorption with respect to Ru(0001) may originate from the transition from the triple bond to the single bond.

Similar to the transition metal surfaces, the CH_2 dehydrogenation kinetics is also mainly determined by its thermochemistry on $Ru_1/TiO_2(110)$. As shown in Figure 3b and Table S6, CH_2 dehydrogenation is the most difficult step among all the dehydrogenation steps, with the ΔE_{act} of 1.29 eV. The result is in sharp contrast with that on Ru(0001) (ΔE_{act} = 0.19 eV), which means that more CH_2 species can be expected on $Ru_1/TiO_2(110)$. We further compare the $2CH_2^* \rightarrow C_2H_4^*$ reaction on Ru(0001) and $Ru_1/TiO_2(110)$, which has been shown to be one of the most possible C−C coupling pathways,[32] and find that the coupling ΔE_{act} on the two surfaces are 1.29 and 0.85 eV, respectively (see Table S7 and Figure S5). Thereafter, the lower CH_2 dehydrogenation activity and higher CH_2 coupling activity on $Ru_1/TiO_2(110)$ not only inhibit coke formation but improve ethylene selectivity.

Besides the improvement in the ethylene selectivity and coke resistance, $Ru_1/TiO_2(110)$ also increases the activity of direct methane conversion that controlled by the first C−H bond scission of methane. Compared with Ru(0001), $Ru_1/TiO_2(110)$ binds CH_4^* stronger by 0.36 eV (smaller ΔG, Figure 4) due to the ligand effect caused by $TiO_2(110)$. To illustrate the ligand effect, surface Ru 4d PDOS for both surfaces without adsorbates are plotted in Figure 7. Compared

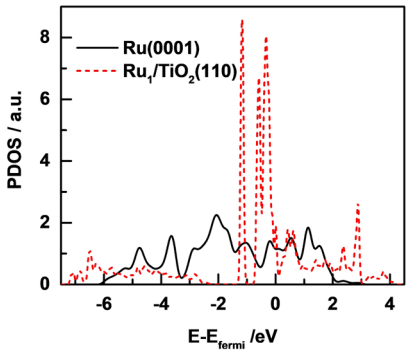

Figure 7. Calculated PDOS for surface Ru 4d orbital of bare Ru(0001) (solid black line) and $Ru_1/TiO_2(110)$ (dashed red line) surfaces.

to Ru(0001), there are considerable states available around the Fermi level for Ru atoms in the $Ru_1/TiO_2(110)$ surface, which would make it more active. Moreover, the larger spatial extension of Ru 4d-orbitals on the $Ru_1/TiO_2(110)$ surface than that on Ru(0001) surface may allow more extensive charge transfer and redistribution, forming a stronger chemical bond with adsorbates accordingly. Compared to CH_4 adsorption, the ligand effect on $Ru_1/TiO_2(110)$ strengthens CH_3 and H adsorption more (Figure 5b), leading to more negative ΔH (by 0.79 eV, Table S6) and lower ΔE_{act1} (by 0.87 eV, Figure 4) for $CH_4^* \rightarrow CH_3^* + H^*$ than on Ru(0001).

The fundamental insights gained can be applied to improve the design principles for catalyst and catalytic process for non-oxidative direct conversion of methane. For instance, nano-structuring and nature of single site and substrate are two possible approaches to improve catalysts as these approaches manipulate the relative adsorption strength of CH_x. In addition, the unfavorable thermochemistry, particularly the effect of entropy for CH_4 adsorption, mainly results in the low activity for non-oxidative direct conversion of methane. The innovation in reaction process by adding suitable oxidants (such as H_2O_2, N_2O, etc.) or superacid can significantly improve the thermochemistry and reduce the reaction temperatures for direct methane conversion.[39−42] The electro-catalytic conversion of methane, which can operate at milder conditions and avoid additional separation of products (H_2 from C_2H_4), also provides a more economical and eco-friendly approach for the direct methane conversion.[43]

4. CONCLUSIONS

Using density functional calculations, the methane adsorption and the relative strength of CH_2 and CH adsorption have been identified as the key factors that affect the activity and selectivity of non-oxidative direct methane conversion on conventional transition metal catalysts. By decreasing coordination number in single Ru sites-embedded $TiO_2(110)$, the adsorption strength of CH_x (x = 0−4) is tuned, particularly CH binding is largely weakened with respect to CH_2, thus leading to increased activity and improved ethylene selectivity and coking resistance. This work offers mechanistic understanding into non-oxidative direct methane conversion at the atomic level, and the surface-coordination-environment-guided catalysts design can potentially be used for direct methane conversion and other important reactions of technological interest.

■ ASSOCIATED CONTENT

Supporting Information

The Supporting Information is available free of charge on the ACS Publications website at DOI: 10.1021/acs.jpcc.9b01638.

Calculated energetic and structures of CH_4 dehydrogenation and CH_2 coupling on pure metal and $Ru_1/TiO_2(110)$; model for the single Ru sites embedded in a rutile $Ru_1/TiO_2(110)$; and *xyz* coordinates for adsorption and transition states on all the surfaces (PDF)

■ AUTHOR INFORMATION

Corresponding Author

*E-mail: hysu@dicp.ac.cn.

ORCID

Xiufang Ma: 0000-0001-9176-0336
Keju Sun: 0000-0001-8791-4646
Wei-Xue Li: 0000-0002-5043-3088
Hai-Yan Su: 0000-0001-9326-9647

Present Address

#J.-X.L.: Department of Chemical Engineering, University of Michigan, Ann Arbor, MI 48109-2136, USA.

Notes

The authors declare no competing financial interest.

DOI: 10.1021/acs.jpcc.9b01638
J. Phys. Chem. C 2019, 123, 14391−14397

■ ACKNOWLEDGMENTS

We thank the finical supports by the Natural Science Foundation of China (21603146, 21872136), the Natural Science Foundation of Shenzhen University (201552, 827-000106), and the "Strategic Priority Research Program" of the Chinese Academy of Sciences (XDA09030101). We thank Guangzong Fang and Xiaoguang Guo from DICP for the fruitful discussion.

■ REFERENCES

(1) McFarland, E. Unconventional Chemistry for Unconventional Natural Gas. *Science* **2012**, *338*, 340−342.
(2) Schwach, P.; Pan, X.; Bao, X. Direct Conversion of Methane to Value-Added Chemicals over Heterogeneous Catalysts: Challenges and Prospects. *Chem. Rev.* **2017**, *117*, 8497−8520.
(3) Majhi, S.; Mohanty, P.; Wang, H.; Pant, K. K. Direct Conversion of Natural Gas to Higher Hydrocarbons: A Review. *J. Energy Chem.* **2013**, *22*, 543−554.
(4) Tang, P.; Zhu, Q.; Wu, Z.; Ma, D. Methane Activation: The Past and Future. *Energy Environ. Sci.* **2014**, *7*, 2580−2591.
(5) Xu, Y.; Bao, X.; Lin, L. Direct Conversion of Methane under Nonoxidative Conditions. *J. Catal.* **2003**, *216*, 386−395.
(6) Guo, X.; Fang, G.; Li, G.; Ma, H.; Fan, H.; Yu, L.; Ma, C.; Wu, X.; Deng, D.; Wei, M.; Tan, D.; Si, R.; Zhang, S.; Li, J.; Sun, L.; Tang, Z.; Pan, X.; Bao, X. Direct, Nonoxidative Conversion of Methane to Ethylene, Aromatics, and Hydrogen. *Science* **2014**, *344*, 616−619.
(7) Morejudo, S. H.; Zanón, R.; Escolástico, S.; Yuste-Tirados, I.; Malerød-Fjeld, H.; Vestre, P. K.; Coors, W. G.; Martínez, A.; Norby, T.; Serra, J. M.; Kjølseth, C. Direct Conversion of Methane to Aromatics in a Catalytic Co-Ionic Membrane Reactor. *Science* **2016**, *353*, 563−566.
(8) Nishikawa, Y.; Ogihara, H.; Yamanaka, I. Liquid-Metal Indium Catalysis for Direct Dehydrogenative Conversion of Methane to Higher Hydrocarbons. *ChemistrySelect* **2017**, *2*, 4572−4576.
(9) Spivey, J. J.; Hutchings, G. Catalytic Aromatization of Methane. *Chem. Soc. Rev.* **2014**, *43*, 792−803.
(10) Lunsford, J. H. Catalytic Conversion of Methane to More Useful Chemicals and Fuels: A Challenge for the 21st Century. *Catal. Today* **2000**, *63*, 165−174.
(11) Song, Y.; Zhang, Q.; Xu, Y.; Zhang, Y.; Matsuoka, K.; Zhang, Z.-G. Coke Accumulation and Deactivation Behavior of Microzeolite-Based Mo/HZSM-5 in the Non-Oxidative Methane Aromatization under Cyclic CH_4-H_2 Feed Switch Mode. *Appl. Catal., A* **2017**, *530*, 12−20.
(12) Tempelman, C. H. L.; Hensen, E. J. M. On the Deactivation of Mo/HZSM-5 in the Methane Dehydroaromatization Reaction. *Appl. Catal., B* **2015**, *176-177*, 731−739.
(13) Ma, D.; Wang, D.; Su, L.; Shu, Y.; Xu, Y.; Bao, X. Carbonaceous Deposition on Mo/HMCM-22 Catalysts for Methane Aromatization: A TP Technique Investigation. *J. Catal.* **2002**, *208*, 260−269.
(14) Ande, C. K.; Elliott, S. D.; Kessels, W. M. M. First-Principles Investigation of C−H Bond Scission and Formation Reactions in Ethane, Ethene, and Ethyne Adsorbed on Ru(0001). *J. Phys. Chem. C* **2014**, *118*, 26683−26694.
(15) Bothra, P.; Pati, S. K. Improved Catalytic Activity of Rhodium Monolayer Modified Nickel (110) Surface for the Methane Dehydrogenation Reaction: A First-Principles Study. *Nanoscale* **2014**, *6*, 6738−6744.
(16) Kokalj, A.; Bonini, N.; Sbraccia, C.; de Gironcoli, S.; Baroni, S. Engineering the Reactivity of Metal Catalysts: A Model Study of Methane Dehydrogenation on Rh(111). *J. Am. Chem. Soc.* **2004**, *126*, 16732−16733.
(17) Kokalj, A.; Bonini, N.; de Gironcoli, S.; Sbraccia, C.; Fratesi, G.; Baroni, S. Methane Dehydrogenation on Rh@Cu(111): A First-Principles Study of a Model Catalyst. *J. Am. Chem. Soc.* **2006**, *128*, 12448−12454.
(18) Kresse, G.; Furthmüller, J. Efficient Iterative Schemes for *Ab Initio* Total-Energy Calculations Using a Plane-Wave Basis Set. *Phys. Rev. B: Condens. Matter Mater. Phys.* **1996**, *54*, 11169−11186.
(19) Kresse, G.; Furthmüller, J. Efficiency of *Ab-Initio* Total Energy Calculations for Metals and Semiconductors Using a Plane-Wave Basis Set. *Comput. Mater. Sci.* **1996**, *6*, 15−50.
(20) Blöchl, P. E. Projector Augmented-Wave Method. *Phys. Rev. B: Condens. Matter Mater. Phys.* **1994**, *50*, 17953−17979.
(21) Kresse, G.; Joubert, D. From Ultrasoft Pseudopotentials to the Projector Augmented-Wave Method. *Phys. Rev. B: Condens. Matter Mater. Phys.* **1999**, *59*, 1758−1775.
(22) Perdew, J. P.; Burke, K.; Ernzerhof, M. Generalized Gradient Approximation Made Simple. *Phys. Rev. Lett.* **1996**, *77*, 3865−3868.
(23) Lide, D. R. *CRC Handbook of Chemistry and Physics*, 85th ed.; CRC Press LLC, 2005.
(24) Diebold, U. The Surface Science of Titanium Dioxide. *Surf. Sci. Rep.* **2003**, *48*, 53−229.
(25) Monkhorst, H. J.; Pack, J. D. Special Points for Brillouin-Zone Integrations. *Phys. Rev. B: Condens. Matter Mater. Phys.* **1976**, *13*, 5188−5192.
(26) Henkelman, G.; Jónsson, H. Improved Tangent Estimate in the Nudged Elastic Band Method for Finding Minimum Energy Paths and Saddle Points. *J. Chem. Phys.* **2000**, *113*, 9978−9985.
(27) Henkelman, G.; Uberuaga, B. P.; Jónsson, H. A Climbing Image Nudged Elastic Band Method for Finding Saddle Points and Minimum Energy Paths. *J. Chem. Phys.* **2000**, *113*, 9901−9904.
(28) Sun, K.; Zhao, Y.; Su, H.-Y.; Li, W.-X. Force Reversed Method for Locating Transition States. *Theor. Chem. Acc.* **2012**, *131*, 1118.
(29) Liu, Z.-P.; Hu, P. A New Insight into Fischer−Tropsch Synthesis. *J. Am. Chem. Soc.* **2002**, *124*, 11568−11569.
(30) Su, H.-Y.; Zhao, Y.; Liu, J.-X.; Sun, K.; Li, W.-X. First-Principles Study of Structure Sensitivity of Chain Growth and Selectivity in Fischer−Tropsch Synthesis Using HCP Cobalt Catalysts. *Catal. Sci. Technol.* **2017**, *7*, 2967−2977.
(31) Ciobîcă, I. M.; Frechard, F.; van Santen, R. A.; Kleyn, A. W.; Hafner, J. A DFT Study of Transition States for C−H Activation on the Ru(0001) Surface. *J. Phys. Chem. B* **2000**, *104*, 3364−3369.
(32) Cheng, J.; Gong, X.-Q.; Hu, P.; Lok, C.; Ellis, P.; French, S. A Quantitative Determination of Reaction Mechanisms from Density Functional Theory Calculations: Fischer−Tropsch Synthesis on Flat and Stepped Cobalt Surfaces. *J. Catal.* **2008**, *254*, 285−295.
(33) Chow, Y. K.; Dummer, N. F.; Carter, J. H.; Williams, C.; Shaw, G.; Willock, D. J.; Taylor, S. H.; Yacob, S.; Meyer, R. J.; Bhasin, M. M.; Hutchings, G. J. Investigating the Influence of Acid Sites in Continuous Methane Oxidation with N_2O over Fe/MFI Zeolites. *Catal. Sci. Technol.* **2018**, *8*, 154−163.
(34) Farrell, B. L.; Igenegbai, V. O.; Linic, S. A Viewpoint on Direct Methane Conversion to Ethane and Ethylene Using Oxidative Coupling on Solid Catalysts. *ACS Catal.* **2016**, *6*, 4340−4346.
(35) Chen, X.; Su, X.; Su, H.-Y.; Liu, X.; Miao, S.; Zhao, Y.; Sun, K.; Huang, Y.; Zhang, T. Theoretical Insights and the Corresponding Construction of Supported Metal Catalysts for Highly Selective CO_2 to CO Conversion. *ACS Catal.* **2017**, *7*, 4613−4620.
(36) Watanabe, T.; Funakubo, H.; Saito, K.; Suzuki, T.; Fujimoto, M.; Osada, M.; Noguchi, Y.; Miyayama, M. Preparation and Characterization of *a*- and *b*-Axis-Oriented Epitaxially Grown $Bi_4Ti_3O_{12}$-Based Thin Films with Long-Range Lattice Matching. *Appl. Phys. Lett.* **2002**, *81*, 1660−1662.
(37) Kattel, S.; Yan, B.; Chen, J. G.; Liu, P. CO_2 Hydrogenation on Pt, Pt/SiO_2 and Pt/TiO_2: Importance of Synergy between Pt and Oxide Support. *J. Catal.* **2016**, *343*, 115−126.
(38) Cui, X.; Wang, B.; Wang, Z.; Huang, T.; Zhao, Y.; Yang, J.; Hou, J. G. Formation and Diffusion of Oxygen-Vacancy Pairs on TiO_2(110)-(1×1). *J. Chem. Phys.* **2008**, *129*, 044703.
(39) Cui, X.; Li, H.; Wang, Y.; Hu, Y.; Hua, L.; Li, H.; Han, X.; Liu, Q.; Yang, F.; He, L.; Chen, X.; Li, Q.; Xiao, J.; Deng, D.; Bao, X. Room-Temperature Methane Conversion by Graphene-Confined Single Iron Atoms. *Chem* **2018**, *4*, 1902−1910.

DOI: 10.1021/acs.jpcc.9b01638
J. Phys. Chem. C 2019, 123, 14391−14397

(40) Williams, C.; Carter, J. H.; Dummer, N. F.; Chow, Y. K.; Morgan, D. J.; Yacob, S.; Serna, P.; Willock, D. J.; Meyer, R. J.; Taylor, S. H.; Hutchings, G. J. Selective Oxidation of Methane to Methanol Using Supported AuPd Catalysts Prepared by Stabilizer-Free Sol-Immobilization. *ACS Catal.* **2018**, *8*, 2567−2576.
(41) Kanitkar, S.; Carter, J. H.; Hutchings, G. J.; Ding, K.; Spivey, J. J. Low Temperature Direct Conversion of Methane Using a Solid Superacid. *ChemCatChem* **2018**, *10*, 5019−5024.
(42) Xu, J.; Armstrong, R. D.; Shaw, G.; Dummer, N. F.; Freakley, S. J.; Taylor, S. H.; Hutchings, G. J. Continuous Selective Oxidation of Methane to Methanol over Cu- and Fe-Modified ZSM-5 Catalysts in a Flow Reactor. *Catal. Today* **2016**, *270*, 93−100.
(43) Xie, S.; Lin, S.; Zhang, Q.; Tian, Z.; Wang, Y. Selective Electrocatalytic Conversion of Methane to Fuels and Chemicals. *J. Energy Chem.* **2018**, *27*, 1629−1636.

DOI: 10.1021/acs.jpcc.9b01638
J. Phys. Chem. C 2019, 123, 14391−14397